Journal of Environmental Chemical Engineering 9 (2021) 105816

Contents lists available at ScienceDirect

Journal of Environmental Chemical Engineering

journal homepage: www.elsevier.com/locate/jece

# Methane decomposition for hydrogen production over biomass fly ash-based $CeO_2$ nanowires promoted cobalt catalyst

Jehangeer Raza [a], Asif Hussain Khoja [a,*], Salman Raza Naqvi [b], Muhammad Taqi Mehran [b], Sehar Shakir [c], Rabia Liaquat [c], Muhammad Tahir [d], Ghulam Ali [c]

[a] Fossil Fuels Laboratory, Department of Thermal Energy Engineering, US-Pakistan Centre for Advanced Studies in Energy (USPCAS-E), National University of Sciences and Technology (NUST), Sector H-12, Islamabad 44000, Pakistan
[b] School of Chemical and Materials Engineering (SCME), US-Pakistan Centre for Advanced Studies in Energy (USPCAS-E), National University of Sciences and Technology (NUST), Sector H-12, Islamabad 44000, Pakistan
[c] Department of Energy Systems Engineering, US-Pakistan Centre for Advanced Studies in Energy (USPCAS-E), National University of Sciences and Technology (NUST), Sector H-12, Islamabad 44000, Pakistan
[d] Chemical Reaction Engineering Group (CREG), School of Chemical and Energy Engineering, Faculty of Engineering, Universiti Teknologi Malaysia (UTM), 81310 Skudai, Johor Bahru, Malaysia

ARTICLE INFO

Editor: V. Victor

*Keywords:*
Methane decomposition
Biomass fly ash
$CeO_2$
$H_2$ production

ABSTRACT

In this work, the biomass fly ash (BFA) was investigated as a potential catalyst for the thermo-catalytic decomposition of methane and attractive approach for hydrogen ($H_2$) production. The BFA based $CeO_2$ nanowires promoted cobalt catalyst was synthesized for catalytic methane ($CH_4$) decomposition and was tested in a fixed bed reactor. The physicochemical properties of the catalyst were investigated using various techniques such as X-ray powder diffraction, scanning electron microscopy, energy-dispersive X-ray spectroscopy, thermal gravimetric analysis, and Fourier transformed infrared. The pure crystalline micro-flake BFA was modified using synthesized $CeO_2$ nanowires and the resulted micro flakes cross-linked with nanowires shown thermal stability up to 900 °C. The high stability of the catalyst makes it suitable for the thermal catalytic decomposition of methane. The activity of the catalyst was tested at 850 °C to analyze the $H_2$ production and $CH_4$ conversion. The obtained results revealed that support and promoter exhibit a strong impact on the $CH_4$ conversion and $H_2$ yield in catalyst screening tests. A maximum conversion of 71% for $CH_4$ with 44.9% $H_2$ yield was recorded for 34 h on stream activity while using 5% Co/$CeO_2$-BFA as the catalyst. While BFA and Co-BFA as catalyst showed 36% and 47% conversion of $CH_4$, respectively which indicates that the addition of promoter shows an increase in values of both conversion of $CH_4$ and $H_2$ yield. Compared to traditional catalyst support, the use of waste-sourced catalyst support for $CH_4$ decomposition provides a greener and more economical route for $H_2$ production.

## 1. Introduction

Currently, the global energy framework is centered on fossil fuels and there are two major challenges associated with the extensive utilization of fossil fuels (i) energy sustainability and (ii) greenhouse gas (GHG) emissions [1,2]. Because of rapid commercialization and urbanization, energy demand is rising day by day and fossil fuels are typically used to meet the growing energy requirement which results in the depletion of resources [3] and releases GHGs emissions [4], especially $CO_2$ which contributes most to global warming [5,6]. Efforts have been taken across the globe to develop renewable, clean, and sustainable sources of energy [7,8]. Such as the utilization of the GHG like $CO_2$ and $CH_4$ for fuels production such as syngas ($H_2$, CO) [9,10], methanol [11] and $H_2$ seek much attention in recent times [9,12]. Currently, researchers are focused on the utilization of syngas for liquid fuel and $H_2$ based fuel cell applications. Fuel cell utilizes $H_2$ for the production of heat and electricity simultaneously which is considered to be the cleaner and cost-effective utilization of $H_2$ [13].

The major challenge associated with the use of $H_2$ fuel cell technology is the lack of availability of "elemental hydrogen" in nature [14]. The $H_2$ is always chemically bonded with other elements and occurs in compound form in nature, such as water, ammonia, and hydrocarbons, etc. Currently, researchers are working on various traditional and renewable technologies for $H_2$ production [15]. Methods that are

* Corresponding author.
*E-mail address:* asif@uspcase.nust.edu.pk (A.H. Khoja).

https://doi.org/10.1016/j.jece.2021.105816
Received 8 January 2021; Received in revised form 27 May 2021; Accepted 3 June 2021
Available online 7 June 2021

devised already for $H_2$ production such as partial oxidation of methane (POM), bio-hydrogen production, steam reforming of methane (SRM), biomass gasification, coal gasification, water splitting, and thermo-catalytic decomposition of methane [16–26]. Currently, for $H_2$ and syngas production, POM and SRM are the state-of-art technologies being practised around the world [25–27]. Although these methods have their limitations in terms of producing $CO_2$, CO, catalyst deactivation and purification of produced $H_2$ [27–30]. However, at the same time production of $H_2$ is highly depended on utilization of fossil fuel because of its availability and well-developed technologies. Among fossil fuels natural gas (NG) is mostly utilized as it consists of more than 85% of $CH_4$, and the processing of agriculture and solid waste also evolve $CH_4$ gas that can be utilized for $H_2$ production which seems a more productive way for sustainable energy routes. The drawbacks of the technologies that directly utilize $CH_4$, mostly for power generation are having lower efficiency and causes $CO_2$ emissions that contribute to global warming [31].

The thermal catalytic decomposition of $CH_4$ for $H_2$ production is one of the cleaner routes as presented in reaction (R1). Owing to its simplest and lightest existence, $H_2$ gets more attention and is known as a clean fuel. The $H_2$ can produce more energy than the parent fuel and do not produce any GHG upon combustion [22,28]. Thermo-catalytic decomposition of $CH_4$ method is used to convert $CH_4$ directly into $H_2$ gas. Thermo-catalytic decomposition of $CH_4$ is an endothermic, single-step and economical process which reduced temperature required for the given process in absence of a catalyst for $H_2$ production. The $H_2$ produced as a result of thermo-catalytic decomposition is almost 100% pure and no further processes for its purification are needed [2]. Carbon nanomaterial formed as a by-product is valuable for many applications because of its interesting properties such as mechanical strength, energy storage capacity and strong resistance towards acids and bases [26,29,32].

$$CH_4 \rightarrow C + 2H_2 \quad \Delta H^{\circ}_{25^{\circ}C} = 75\text{kJmol}^{-1} \text{ (methane decomposition)} \qquad \text{(R1)}$$

Methane is a stable hydrocarbon and requires a high reaction temperature (1000–1200 ℃) for its decomposition in the absence of the catalyst. Therefore, a suitable catalyst with desirable properties is used to decompose $CH_4$ molecules into $H_2$ and carbon at a relatively lower temperature [30,33]. Various studies were conducted on Ni, Fe, Co and noble metal loaded catalyst over conventional support like $Al_2O_3$ [34], $SiO_2$ [22], MgO [35], $ZrO_2$ [27], $La_2O_3$ [36], $TiO_2$ [37] etc for of $CH_4$ decomposition. However, the economics and preparation of such support material are major concerns and seek alternative routes. Diversified approaches such as bi-metallic, tri-metallic and co-supported catalyst were used to get promising results for the thermo-catalytic decomposition of $CH_4$ [31,38]. Among the metal loaded catalysts, Ni loaded catalyst is mostly investigated for $CH_4$ decomposition due to some excellent properties such as lower activation temperature and high initial $H_2$ output, but still facing some major limitations in terms of sintering, carbon deposition, catalyst deactivation [38,39] and its instability at elevated temperature which has a strong effect on $CH_4$ conversion and $H_2$ yield [40]. Cobalt-based catalyst is another suitable and competitive candidate for $CH_4$ decomposition in elevated temperatures. Various cobalt-base catalysts were used with excellent catalytic performance and stability even at higher temperatures [38]. The catalytic performance of heterogeneous catalyst usually depends on the method of preparation, type of active metal used, support material, its structure and presence of promoter [38,41].

Generally, support has a major role in the catalytic activity of catalyst because it is responsible for smoothening the path for metal dispersion, metal-support interaction and exposure of active sites [39,42]. However, the economics and complex method for the preparation of such support material is the main problem. To overcome these challenges, various approaches and processes were applied for the synthesis of support material from waste materials, such perspectives seeking attention due to its low cost, and renewable sources [43,44].

The solid fuel-fed power plants produce a massive amount of both types of ash i.e bottom ash and fly ash, and its disposal is a main environmental challenge [45]. Ash is usually dumped at waste landfill sites which is not cleaner disposal, and it may harm human health. At present, there has been an interest in the sustainable management of waste fly ash to optimize waste material recovery. Coal fly ash, for example, is used for road construction, cement production, zeolite preparation and other building materials such as concrete [46]. The detailed coal fly ash analysis confirms the existence of various metal oxides, including $Al_2O_3$, $Fe_2O_3$, $SiO_2$and MgO [47]. The presence of metal oxides makes it very reasonable to use them as a catalyst support material for various reforming applications. Coal ash-supported Ni-base catalyst was used by steam reforming of acetic acid and phenol for hydrogen production. The results show that the conversion of reactants and production of $H_2$ were improved due to the presence of metal oxides in coal ash [48]. The coal ash as catalyst was used in steam gasification of palm shell for production of $H_2$ and syngas and have shown some promising results due to the presence of metal oxides in ash and its suitable textural properties [49]. Similarly, the ash from various solid fuels and waste such as coal, refuse-derived fuel and waste rubber tires were tested as catalysts supports for the production of $H_2$ in the biomass steam reforming process and the results were very encouraging as the metal oxides and morphology contributed to the reforming process [50]. The studies show that biomass fly ash (BFA) also has metal oxides such as $Al_2O_3$, $Fe_2O_3$, $SiO_2$, MgO, $CaCO_3$ and $K_2O$ and desirable morphology for catalytic applications in several reforming technology [45]. Instead of the desirable physiochemical properties, BFA was constantly overlooked to be used as a catalyst in the literature. The goal and motivation of this study is to investigate and use cobalt loaded BFA for the thermo-catalytic decomposition of methane that will assists in the sustainable management of BFA and also reduce the costs and efforts required for complex methods to prepare conventional support materials.

Typically, the promoter helps to increase metal dispersion over the support, catalyst stability and alter the morphology of deposited carbon [35]. Cerium oxide ($CeO_2$) has distinctive redox properties that influence the catalyst physicochemical properties and increase the active metal dispersion over support, further reducing the sintering of active metals. Previously $CeO_2$ was used to produce syngas via partial oxidation of methane [51] and dry reforming of methane [52] with promising catalytic activity and selectivity. Recently, $CeO_2$ was used for thermo-catalytic decomposition of methane, where it not only improves catalytic activity and stability but also has good interaction with transition metals and provides better dispersion of metal over support [53].

In this work, two environmental concerns such as $CH_4$ and BFA were considered to make a sustainable route for $H_2$ production. The Co loaded $CeO_2$ promoted catalyst prepared for thermocatalytic decomposition of methane. For this purpose, $CeO_2$ nanowires were prepared by conventional hydrothermal method and cobalt loaded over BFA support catalyst via wetness impregnation method. The prepared catalyst Co/$CeO_2$-BFA is characterized using X-ray powder diffraction (XRD), scanning electron microscopy (SEM), energy-dispersive X-ray spectroscopy (EDS), thermogravimetric analysis (TGA) and Fourier transformed infrared spectroscopy (FTIR). The catalyst performance was carried out in a fixed bed reactor and assessed in terms of $CH_4$ conversion, $H_2$ selectivity and yield. Moreover, the catalyst activity was tested for 34 h to analyze the stability of the catalyst and its evolution in high-temperature reaction. Finally, the spent catalyst was also characterized by XRD, SEM, EDX and TGA to investigate the physicochemical changes and carbon formed over the catalyst surface.

## 2. Experimental

### 2.1. Preparation of Co/$CeO_2$-BFA

The biomass fly ash (BFA) was obtained from a local biomass-fired

power plant. The BFA preparation scheme is presented in Fig. 1. BFA samples were washed with deionised (DI) water prepared by drying in an oven for 10 h at 120 ℃ to remove moisture and then grinded and sieved to achieve the fine powder. BFA was calcined at 800 ℃ for 3 h to improve its crystallinity and to remove the unburnt carbon and alkaline material.

$CeO_2$ was synthesized by the hydrothermal process as shown in Fig. 1. Cerium (III) nitrate hexahydrate (Sigma Aldrich, 99.99%, USA) ($Ce(NO_3)_3{\cdot}6H_2O$) was added to the required amount of DI water to prepare a solution (0.1 M) maintaining pH at 10.0, stirred for 15 min at 60 ℃ to make the homogenous nitrate solution. The homogenous nitrate solution was then shifted to a 200 mL Teflon lined stainless steel autoclave (China) for the hydrothermal process. The autoclave was kept in the furnace for the hydrothermal process for 24 h at 160 ℃ and then cooled to room temperature naturally. The sample was rinsed several times with DI water and absolute ethanol (ACS reagent 99.5%) to remove impurities and maintain pH at 7.0. The sample was dried for 10 h in an oven at 120 ℃ and trailed by calcination (800 ℃) for 3 h.

The $Co/CeO_2$-BFA catalyst was formulated by the incipient wetness impregnation method [54,55]. BFA and $CeO_2$ powders were added to the DI water and kept for 15 min on stirring at 60 ℃. Cobalt (II) nitrate hexahydrate ($Co(NO_3)_2{\cdot}6H_2O$) (Merck, 99.99%, USA) solution (0.1 M) was prepared using DI water and heated at 60 ℃ for 10 min with continuous stirring. The required amount of BFA and $CeO_2$ nano powder was added to the precursor solution and was stirred at 110 ℃ for 3 h. The sample was dried overnight in an oven at 110 ℃, then grinded and performed calcination at 700 ℃ for 3 h.

### 2.2. Catalyst characterization

The physicochemical properties of the catalyst were analyzed employing a variety of methods i.e. XRD, SEM, TGA and FTIR spectroscopy. The catalyst crystal structure was determined using an X-Ray diffractometer, D8 Advance (Bruker Advanced, Germany) scanning from 05° to 80° using a step size of 0.05°/5 s. X-ray diffractometer characterized with DIFFRAC plus EVA version 5.0, Bragg-Brentano configuration, scintillation detector and 1.5418 Å wavelength radiations were used to determine the crystallinity of the material. The catalyst crystallite size is calculated using the Scherrer equation [55,56].

The morphology and elemental distribution of the fresh and spent catalyst were studied using SEM (JSM-6490A JEOL Japan) with a resolution power of 3 nm at 30 kV with an extension of 10–200,000X to achieve the desirable micrograph of material. Elemental composition assessment of the fresh nanocomposite and spent catalyst was performed with EDX detector (Oxford Instruments, model: 51-AD0007).

Thermal stability analysis was performed by thermal gravimetric analyser TGA 5500 TA Instruments. The samples were heated from 25 ℃ to 900 ℃ at a heating rate of 10 ℃ $min^{-1}$ in $N_2$ environment with a flow rate of 25 mL $min^{-1}$ to study the thermal stability of the catalyst sample. The air environment was adopted for the spent catalyst analysis with the same experimental conditions. FTIR spectroscopy was conducted to determine the functional group and interaction between Co- and Ce employing Cary 630 FTIR (Agilent Technologies USA). FTIR spectrum with the resolution of 2 $cm^{-1}$ and wavenumber in the range 650–4000 $cm^{-1}$ was recorded.

### 2.3. Experimental setup for methane cracking

Methane decomposition reaction was carried out in a fixed bed thermal reactor (Parr Instrument, 5401, USA) with a continuous flow of gases shown in Fig. 2. The thermal reactor consisting of a fixed bed stainless steel (SS 316) reactor having inner diameter ID = 12 mm and length of 300 mm with single zone heating furnace was used. The pressure gauge (2.5 bar) is installed to monitor the pressure in the reactor. The prepared nanocatalyst was stacked in the middle of the SS reactor tube sandwiched using quartz wool. The $CH_4$ (99.99%) flow rate was regulated by a mass flow controller (Brooke instruments, USA). The temperature of the thermal reactor was controlled by a process controller (4871, Parr Instrument). The temperature and flow were monitored using an online SCADA system. The condenser was used to remove any moisture and supplied dry gases for analysis. The $CH_4$ fed and $H_2$ yield were evaluated using a gas chromatograph (GC-TCD) (GC-2010 Plus, Shimadzu Japan) equipped with a thermal conductivity detector (TCD). The TCD is furnished with a capillary column (RT-MS5A, 30 m x 0.32 mm ID, 30 μm) used to detect $CH_4$ and $H_2$ [45].

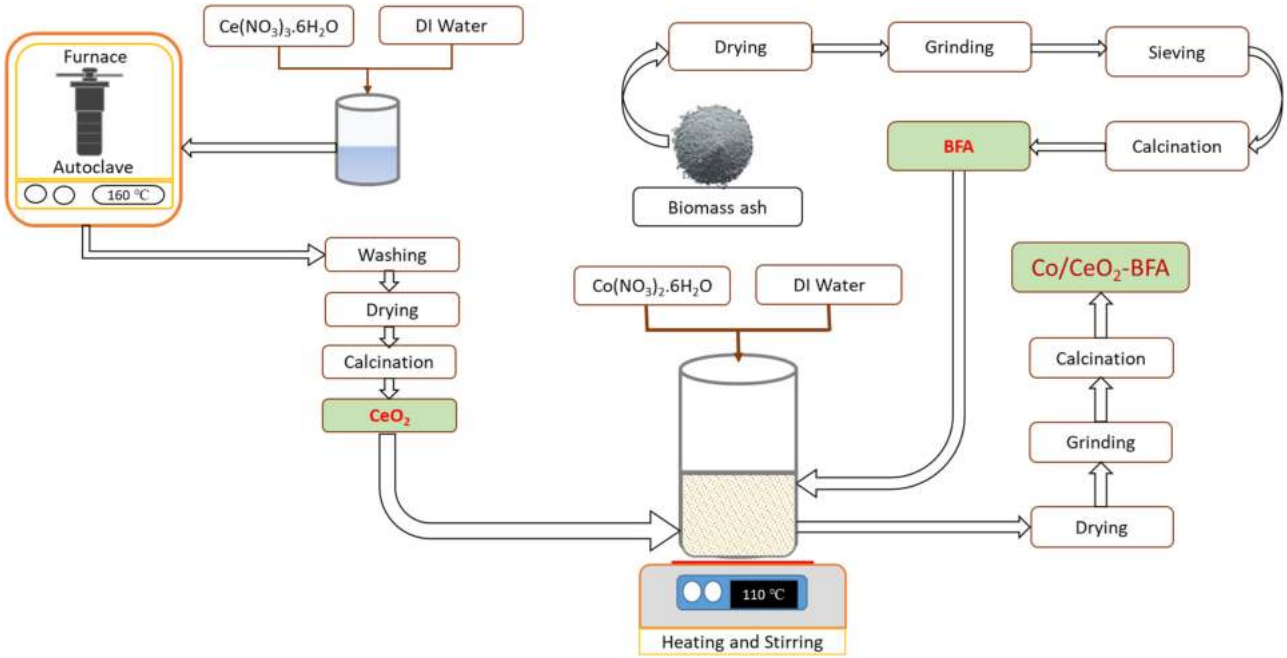


**Fig. 1.** Schematic of $Co/CeO_2$-BFA synthesis.

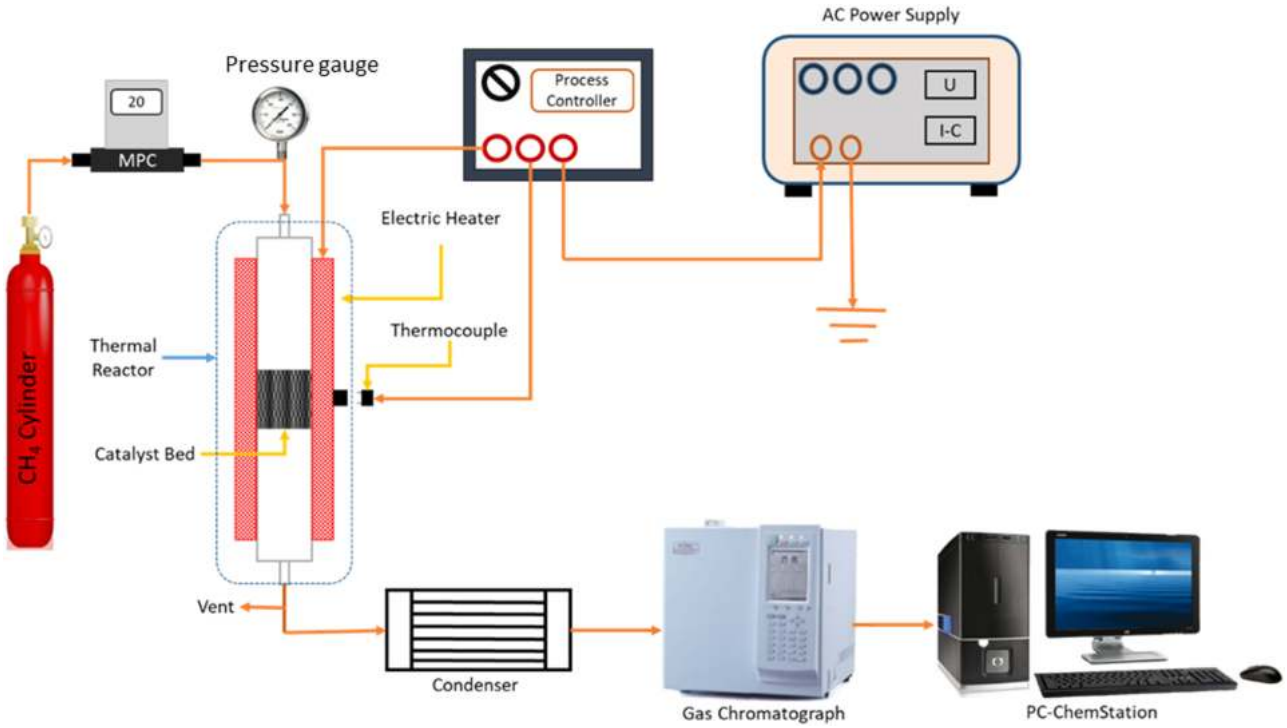


**Fig. 2.** Schematic of the experimental setup for catalytic methane decomposition.

### 2.4. Methane decomposition activity

The catalytic decomposition of methane was examined for $CH_4$ conversion, the $H_2$ selectivity and yield is given in Eqs. (1–3).

$$CH_4 \text{ conversion } (X_{CH_4})\% = \left[\frac{(n\ CH_4)_{converted}}{(n\ CH_4)_{feed}} \times 100\right] \quad (1)$$

$X_{CH4}$ is the conversion of methane, $n(CH_4)_{converted}$ the number of moles of methane converted and $(nCH_4)_{feed}$ is moles of methane at the inlet of the reactor.

$$H_2 \text{ selectivity } (S_{H_2})\% = \left[\frac{(nH_2)_{produced}}{(2 \times nCH_4)_{converted}} \times 100\right] \quad (2)$$

$$H_2 \text{ yield } (Y_{H_2})\% = \left[\frac{(nH_2)_{produced}}{2 \times (nCH_4)_{feed}} \times 100\right] \quad (3)$$

An analytical approach has been used to calculate the possible carbon formed inside the reactor over 34 h TOS. The weight of the deposited carbon over the reactor surface were calculated by subtracting weight of the catalyst loaded reactor before reaction from the weight of the reactor after completion of the reaction for stability analysis as shown in Eq. (4).

$$Carbon\ formed\ (g) = \left[\left(\text{Reactor weight}_{(post-reaction)}\right) - \left(\text{Reactor weight}_{(pre-reaction)}\right)\right] \quad (4)$$

## 3. Results and discussion

### 3.1. Physicochemical properties of the catalyst

For the structural investigation of the BFA, $CeO_2$, and 5%Co/$CeO_2$-BFA, XRD experiments were performed, and the patterns are shown in Fig. 3 and calculated values are listed in Table 1. The XRD pattern of BFA exhibits diffraction peaks for the different crystalline phases. The key diffraction peak at 2θ with a value of 25.4° indexed directly to orthorhombic $CaSO_4$ (JCPDS# 37-1496) with phase (020) [57]. The $CaCO_3$

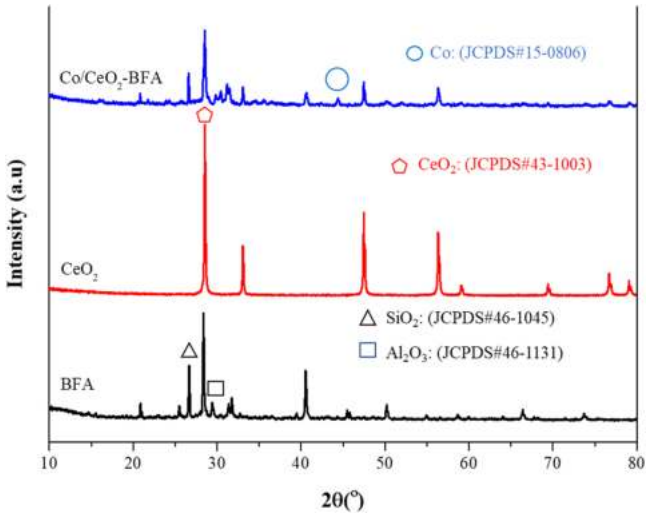


**Fig. 3.** XRD analysis of BFA, $CeO_2$, and 5%Co/$CeO_2$-BFA.

**Table 1**
JCPDS card, 2$\theta$ values, and *hkl* values of different phases in XRD analysis.

| Catalyst | Compound | JCPDS # | 2θ (°) | *(hkl)* | *Crystallite size (nm)* |
|---|---|---|---|---|---|
| BFA | MgO | 45-0946 | 44 | *(211)* | *16.5* |
| | $CaCO_3$ | 47-1743 | 29.4 | *(104)* | *20.6* |
| | $SiO_2$ | 46-1045 | 26.5 | *(101)* | *8.9* |
| | $Fe_2O_3$ | 16-0653 | 32.8 | *(220)* | *10.9* |
| | $Al_2O_3$ | 46-1131 | 30.3 | *(020)* | *13.6* |
| $CeO_2$ | $CeO_2$ | 43-1002 | 28.5 | *(111)* | *9.1* |
| 5%Co/$CeO_2$-BFA | Co | 15-0806 | 44.2 | *(111)* | *9.6* |

(JCPDS# 47-1743) with phase (104) is detected at $2\theta = 29.4^{\circ}$ [58]. The diffraction peak of $SiO_2$ (JCPDS# 46-1045) with phase (101) have been estimated at $2\theta = 26.5^{\circ}$ [59]. The $Fe_2O_3$ major diffraction peak was observed at $2\theta = 32.8^{\circ}$ for the cubic structure of (JCPDS# 16-0653) with phase (220) [60]. $Al_2O_3$ (JCPDS# 46-1131) with phase (020) was identified at an $2\theta = 30.3^{\circ}$ [61]. The cubic structure MgO (JCPDS N# 45-0946) major peak found at $2\theta = 44^{\circ}$ and phase (211).

For $CeO_2$ (JCPDS# 43-1002) with hkl (111), which indexed explicitly face-centered cubic crystalline phase was observed at $2\theta = 28.5^{\circ}$ [33]. The cobalt-loaded composite shows an extra major peak with $2\theta = 44.2^{\circ}$ for the face-centered cubic phase of Co (JCPDS# 15-0806) with hkl (111) [62]. Hence, XRD results confirm the synthesis of the high crystalline nanocatalyst with the presence of $CeO_2$, Co, and other metal oxides [63]. The average crystallite size for the BFA is 13.8 nm while $CeO_2$ and Co show 9.1 nm and 9.6 nm respectively.

The morphological structures of BFA, $CeO_2$, and 5%Co/$CeO_2$-BFA nanocomposite were analyzed by using SEM as shown in Fig. 4 with a magnification of 5.0 μm and 1.0 μm. The BFA shows micro flakes-like morphology [45] as depicted in Fig. 4(a,b). Higher magnification shows porosity in the micro-flakes which give crusty behavior to the

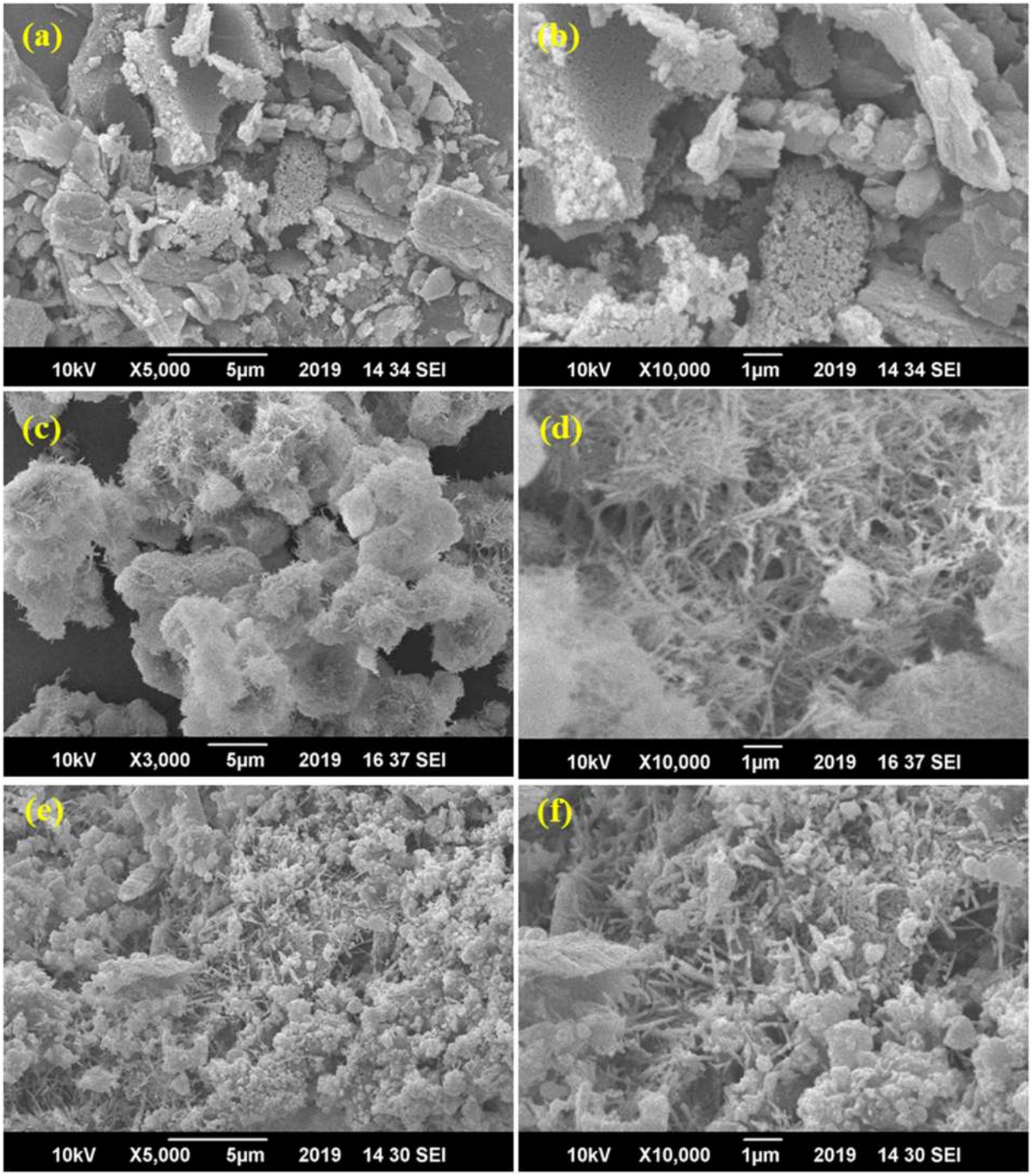


**Fig. 4.** SEM micrographs of synthesized catalyst (a,b) BFA, (c,d) $CeO_2$ nanowires, and (e,f) 5%Co/$CeO_2$-BFA.

catalyst. Micro flakes like structures with porosity are considered arguably excellent for catalytic application due to better dispersion of active metals and interaction with promoters [33]. The $CeO_2$ demonstrates nanowire structure as shown in Fig. 4(c,d) with different magnifications. The $CeO_2$ nanowires are interconnected and formed a complex web-like structure. The wet impregnation method of Co along with the incorporation of $CeO_2$ and BFA is shown in Fig. 4(e,f). The improved dispersion of the Co on the BFA due to micro flakes structure and porosity of support material is evident [22]. The 5%Co/$CeO_2$-BFA nanocomposite clearly shows the infusion of $CeO_2$ nanowires in BFA and improves Co dispersion to achieve higher active sites for methane activation.

The EDS analysis of 5%Co/$CeO_2$-BFA is shown in Fig. 5. The elemental analysis indicates clear peaks for Co, Ce is seen in the EDX spectrum. The spectrum also shows peaks for Ca, Si, Fe, and Al which are the main constituent of the BFA as confirmed in XRD analysis.

The thermal stability of the prepared BFA, $CeO_2$, and 5%Co/$CeO_2$-BFA samples is presented in Fig. 6. TGA profile of BFA in Fig. 6(a) indicates a total of 15% weight loss. The total weight loss of BFA eventuates in three steps. In the first step, up to 150 ℃ temperature, the moisture content of the BFA dried up and count for minute weight loss. In the temperature range of 150–400 ℃, the other volatile matter present in BFA evaporated and is accountable for weight loss in the second phase of the TGA profile. In the third step, major weight loss occurs for the oxidation of organic material and the transfer of Si and Fe phases in temperature ranges from 550 to 900 ℃ [64]. Fig. 6(b) portrays the thermal stability of $CeO_2$ nanowires, which distinctly shows the evaporation of the moisture content from synthesized $CeO_2$ and does not indicate any further weight loss and ascribing to the stability of $CeO_2$ nanowires [65,66]. The TGA profile of the 5%Co/ $CeO_2$-BFA nanocomposite is depicted in Fig. 6(c). The TGA profile portrays a total of 5.5% weight loss up to 750 ℃. The weight loss is related to the release of moisture, volatile content from the material and possible breakdown of carbonates. The weight loss in the final nanocomposite has reduced as compared to the BFA which reveals that Co and $CeO_2$ loading over BFA change the structure and morphology of the nanocomposite as well as strengthen the thermal stability [67].

The functional groups (qualitative analysis) in the range of 4000–650 $cm^{-1}$ wavenumber were determined for BFA, synthesized $CeO_2$ nanowires and 5%Co/$CeO_2$-BFA nanocomposite are presented in Fig. 7(a–c). The weak transmittance peak band in 2500–2000 $cm^{-1}$ shows the physical presence of the OH bond due to the presence of water [68]. While the band below 700 $cm^{-1}$ are indicating Ce-O stretching

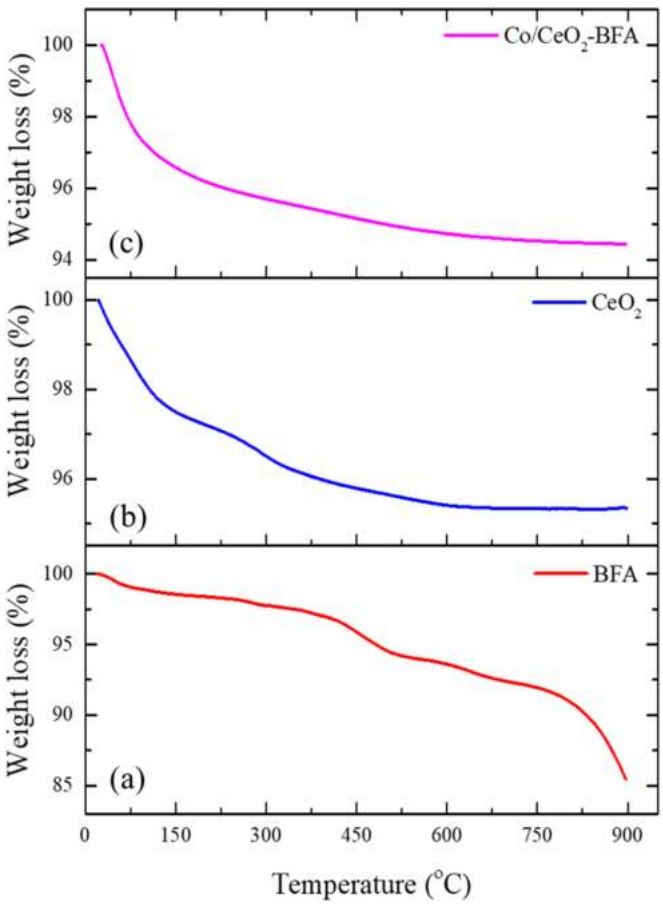


**Fig. 6.** TGA profile of fresh (a) BFA, (b) $CeO_2$ nanowires, and (c) 5%Co/$CeO_2$-BFA.

vibration in the case of $CeO_2$ and nanocomposite [69–71]. The BFA, FTIR spectrum shows obvious bands at 1418 $cm^{-1}$ and 882.36 $cm^{-1}$ which illustrates the stretching vibration of the asymmetric C=O, which confirms the presence of carbonate compound in BFA, while the band at 1110 $cm^{-1}$ demonstrates the Si-O stretching vibration [45,72,73]. The symmetric stretching vibration for Si-O-Al have been observed at a relatively smaller neck at 743.9 $cm^{-1}$ [73]. The stretching modes for 5%

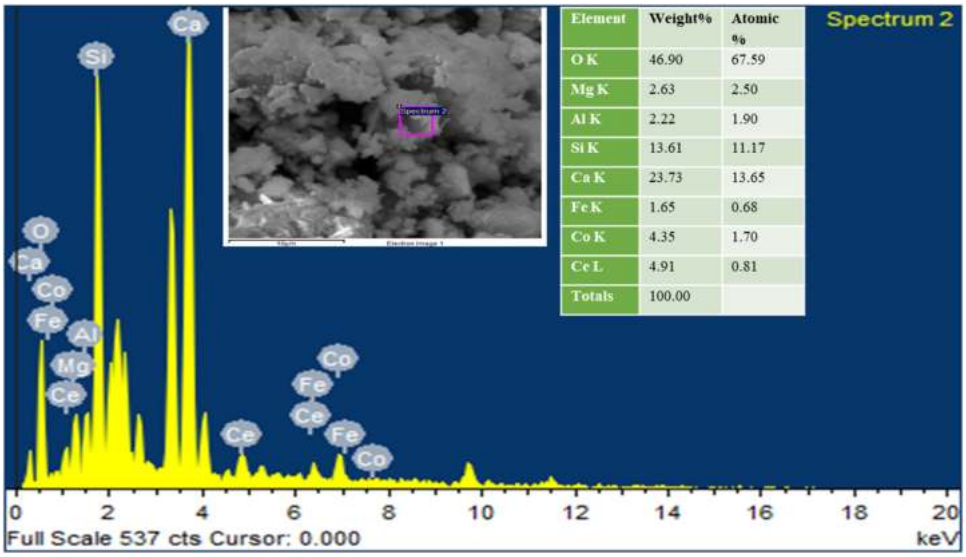


**Fig. 5.** EDX analysis of fresh 5%Co/$CeO_2$-BFA.

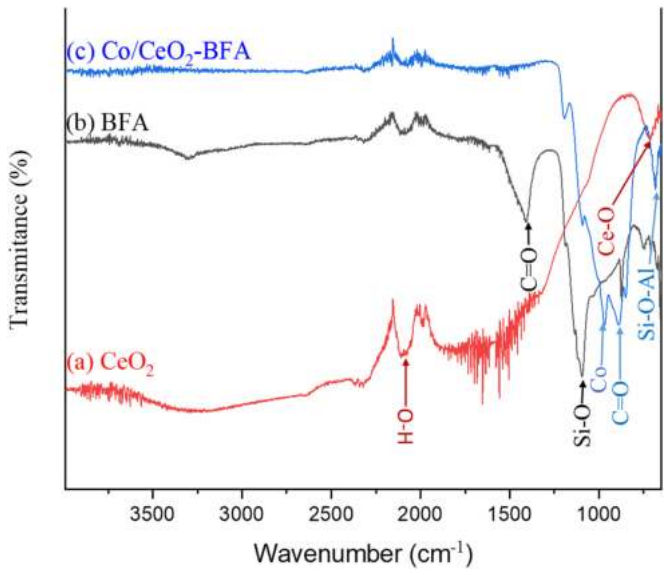


**Fig. 7.** FTIR spectroscopy of fresh (a) $CeO_2$, (b) BFA and (c) 5 wt%Co/$CeO_2$-BFA.

Co/$CeO_2$-BFA at 955.6 $cm^{-1}$ represents C-O vibrations [74]. The band at 1075 $cm^{-1}$ wave number is attributed to Co present in the nanocomposite [75,76].

### 3.2. Catalyst screening test

The catalytic activity of BFA, 5%Co/BFA and 5%Co/$CeO_2$-BFA are screened in terms of $CH_4$ conversion, $H_2$ selectivity and yield as presented in (Fig. 8), while keeping experimental parameters constant; reaction temperature 850 °C, a $CH_4$ flow rate of 20 mL $min^{-1}$ and catalyst loading was 0.5 g. All the reported values for $CH_4$ conversion, $H_2$ selectivity and $H_2$ yield are the average values after the catalyst gain stability. Fig. 8(a) presented the $CH_4$ conversion (28%) for BFA as a catalyst, however, the addition of the Co to BFA increases up to 46% $CH_4$ conversion. It is attributed to the Co active sites and stimulates the $CH_4$ molecule to decompose into carbon and $H_2$ while in the case of BFA, the only supported without activation [77]. Furthermore, the addition of $CeO_2$ as a promoter to Co/BFA raises the $CH_4$ conversion to 71%, since $CeO_2$ improves the Co dispersion over the BFA and also improve metal-support interaction [30].

Fig. 8(b) reveals $H_2$ selectivity for BFA (33.5%), 5%Co/BFA (44%) and 5%Co/$CeO_2$-BFA (62%) respectively. The $H_2$ yield for BFA, 5%Co/BFA and 5%Co/$CeO_2$-BFA corresponds to values 20%, 31% and 44% respectively (Fig. 8(c)). The $H_2$ yield improvement is evidence of the Co and $CeO_2$ interaction with BFA and activation of $CH_4$. The $CH_4$

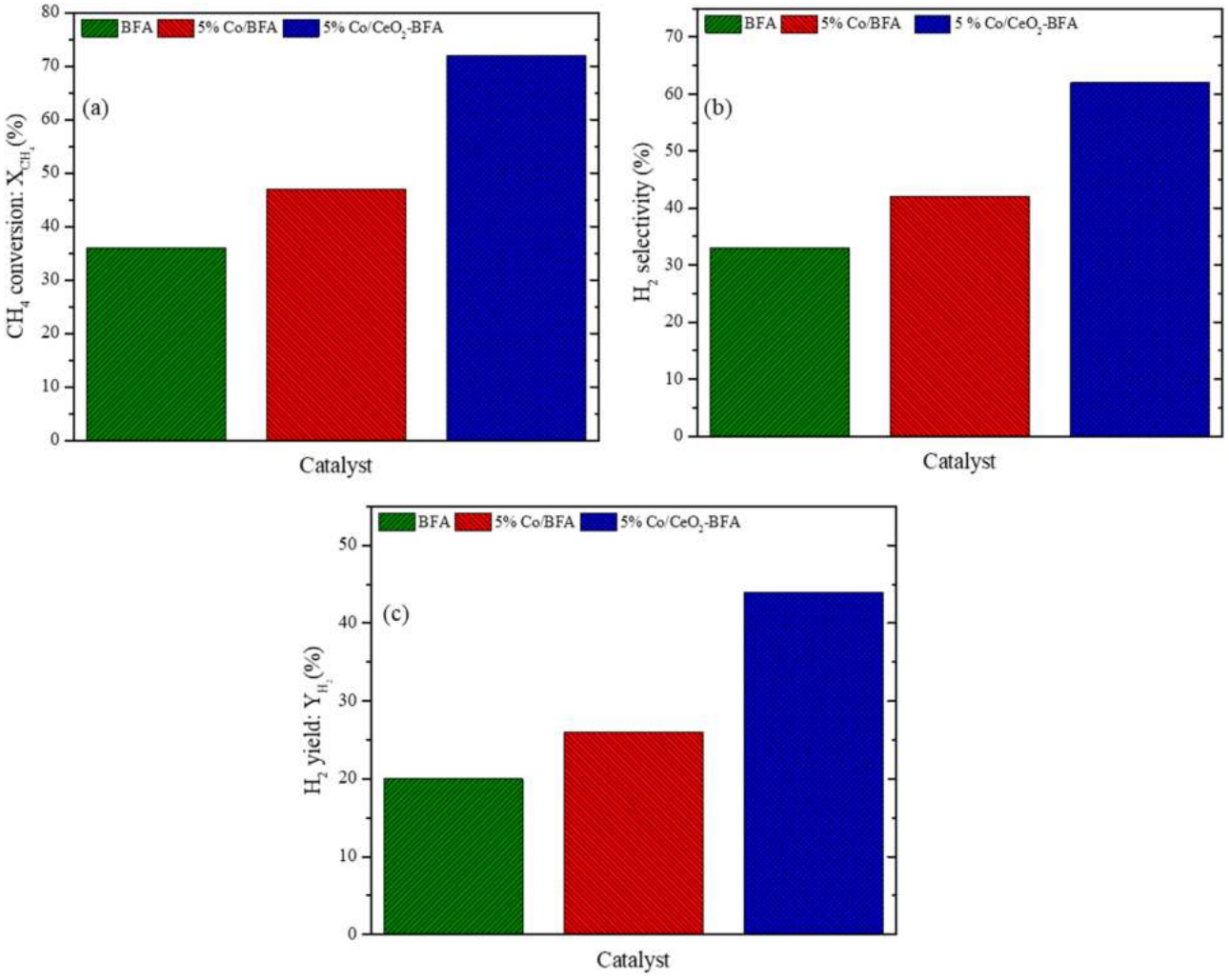


**Fig. 8.** Catalyst screening (a) $CH_4$ conversion, (b) $H_2$ selectivity and (c) $H_2$ yield at reaction temperature = 850 °C, catalyst loading = 0.5 g and $CH_4$ flow rate = 20 mL $min^{-1}$.

conversion enhanced along with $H_2$ selectivity and yield is also attributed to the redox properties of ceria and high mobility of lattice oxygen [78]. In the product analysis, the traces of CO and $CO_2$ were analyzed in the process. Furthermore, ceria also assists in metal-support interaction in a reductive environment. The electrons on the 4*f*-suborbital usually increase the electron density around the Co metal and increase the methane decomposition [79]. The BFA also includes Fe, Al and Si which can also assist in the Co exsolution process rather than suppressing the active sites.

### 3.2.1. *Effect of $CeO_2$ loading over 5%Co-BFA*

The catalytic activity for different loading of $CeO_2$ nanowires as a promoter over 5% Co/BFA catalyst was investigated for $CH_4$ decomposition at a temperature of 850 ℃, a total flow rate of 20 mL $min^{-1}$ and catalyst loading of 0.5 g. Fig. 9 depicts the $CH_4$ conversion, $H_2$ selectivity and yield were enhanced by increasing $CeO_2$ loading in 5%Co/BFA. The $CH_4$ conversions are shown in Fig. 9(a) which displays that 53% of $CH_4$ conversion for 2.5% $CeO_2$ loading and increased to 71% for 5% $CeO_2$ loading. This is due to the $CeO_2$ nanowire structure which gives better metal dispersion, preventing active metal sintering and improving catalyst stability at higher temperatures, but the potential increase in $CeO_2$ loading from 7.5% to 10% increased conversion from 73% to 76%, respectively, because increasing $CeO_2$ loading allows pores to be filled and contributes to $CeO_2$ agglomeration that blocks active sites [30,53]. The identical behavior was evaluated for $H_2$ selectivity and yield. The recorded $H_2$ selectivity values for 2.5%, 5%, 7.5% and 10% of $CeO_2$ loading over Co/BFA catalyst are 46%, 62%, 65% and 66.5% respectively (Fig. 9(b)). While Fig. 9(c) demonstrates $H_2$ yield of 28%, 44%, 47% and 49% respectively for 2.5%, 5%, 7.5% and 10% loading of $CeO_2$. Therefore, the catalyst with 5% $CeO_2$ loading resulted in improved $CH_4$ conversion, $H_2$ selectivity, and yield. Again, the redox properties of $CeO_2$ also support activating the Fe along with Co and expand along with carbon tubes.

### 3.2.2. *Effect of feed flow rate*

The catalytic activity depends heavily on the methane flow rate, as the flow rate determines the gas contact time with the catalyst and at high temperatures in the reactor [23]. Over 5% Co/$CeO_2$-BFA catalyst, $CH_4$ conversion, $H_2$ selectivity and yield at different flow rates were studied while keeping the remaining experimental parameters constant. Experimental findings show that $CH_4$ conversion of 74% at 10 mL $min^{-1}$ was significantly reduced to 60% at 40 mL $min^{-1}$ flow rate as shown in Fig. 10(a). The high concentration of the gas reduces the interaction between the gas molecules and active sites on the catalyst surface [80]. Also, the high concentration contributes to the formation of radicals like $CH_3$, $CH_2$ and CH, and the decomposition of methane could stop as a result of high concentration and other CxHx gases can form [81]. A similar tendency was observed for hydrogen selectivity and yield. The

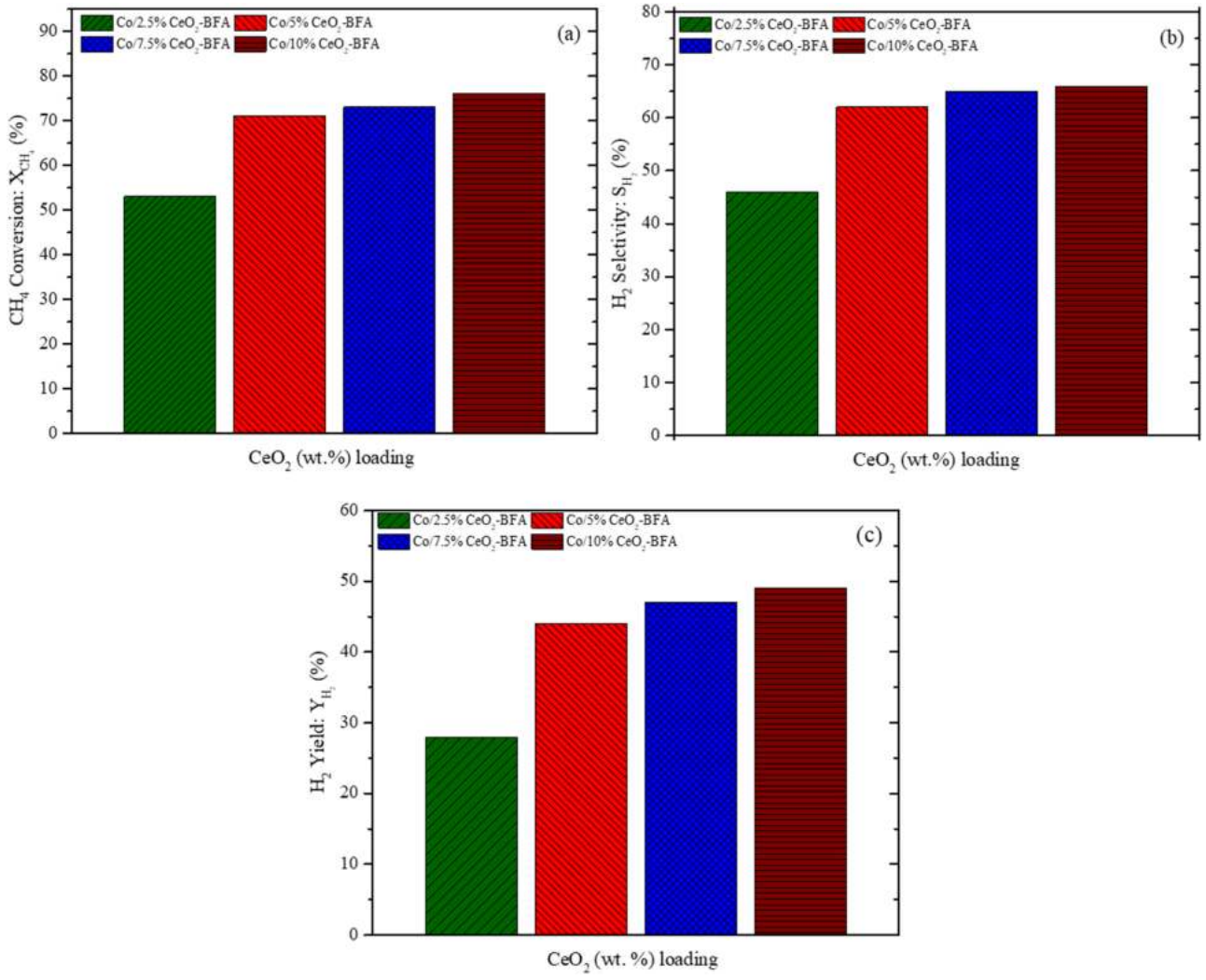


**Fig. 9.** Effect of $CeO_2$ loading on (a) conversion of $CH_4$, (b) selectivity of $H_2$ and (c) $H_2$ yield at reaction temperature = 850 °C, catalyst loading = 0.5 g, and $CH_4$ flow rate = 20 mL $min^{-1}$.

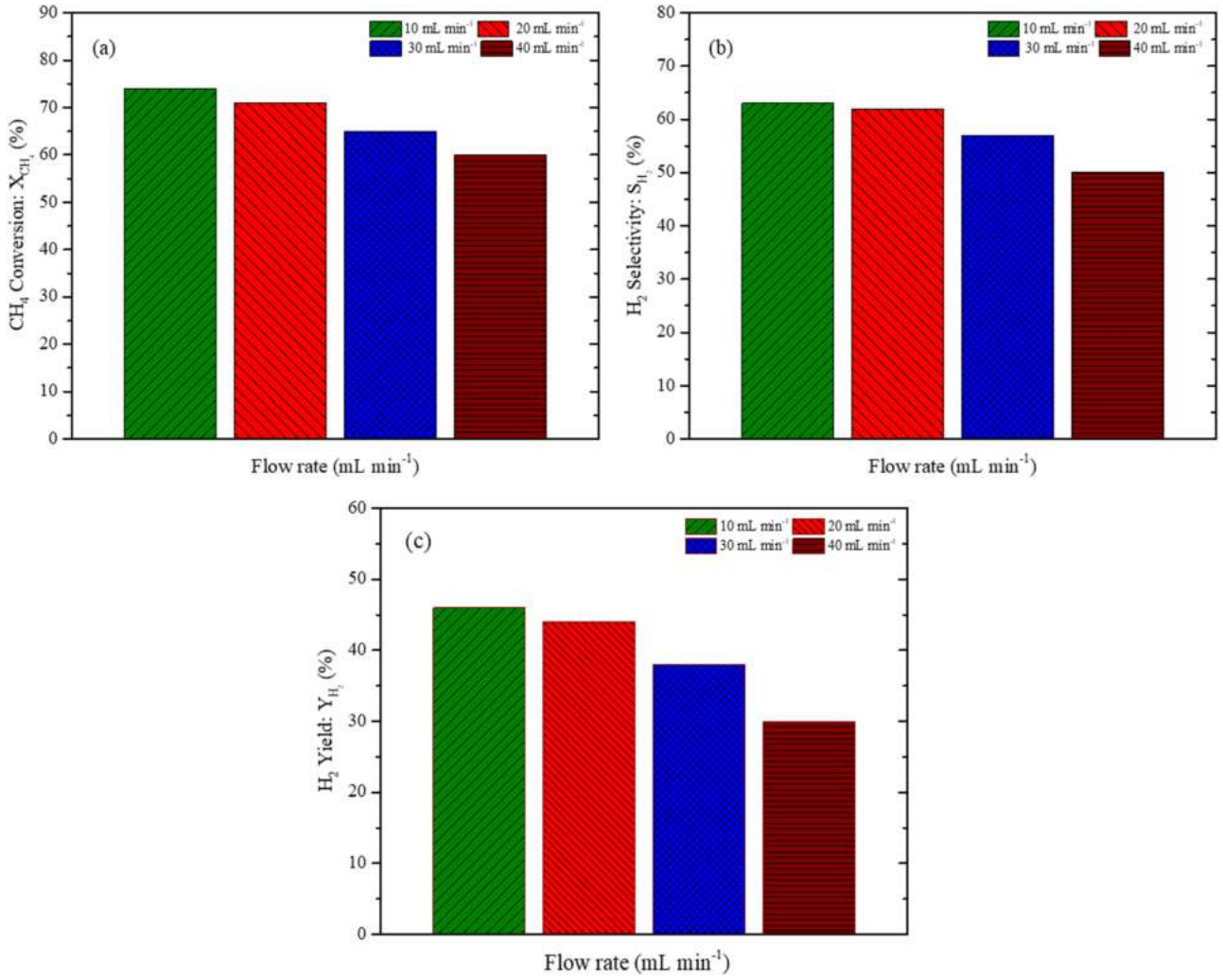


**Fig. 10.** $CH_4$ flow rate effect on (a) conversion of $CH_4$, (b) $H_2$ selectivity and (c) $H_2$ yield at reaction temperature = 850 °C and catalyst loading = 0.5 g.

$H_2$ selectivity is depicted in Fig. 10(b), with values of 63%, 62%, 57% and 50% while keeping flow rate at 10 mL $min^{-1}$, 20 mL $min^{-1}$, 30 mL $min^{-1}$ and 40 mL $min^{-1}$ are noted respectively. In very similar manner, $H_2$ yield of 46%, 44%, 38% and 30% were recorded respectively for flow rate of 10 mL $min^{-1}$, 20 mL $min^{-1}$, 30 mL $min^{-1}$ and 40 mL $min^{-1}$. The flow rate is corresponding to the residence time, increasing the flow rate reduces the residence time and the interaction between the gas molecules and active sites are minimum, thus conversion of $CH_4$ is reduced [55,82].

### 3.2.3. *Stability analysis of 5% Co/$CeO_2$-BFA*

The stability analysis was performed for the 5%Co/5%$CeO_2$-BFA catalyst with respect to time on stream. The analysis was carried at constant experimental parameters i.e. $CH_4$ flow rate of 20 mL $min^{-1}$, 0.5 g catalyst loading and reaction temperature 850 °C. The catalytic activity in terms of $CH_4$ conversion, $H_2$ selectivity and yield is calculated at a time interval of 15 min for the total time of 34 h. Initially, the catalytic activity was very low, due to the reason that produced $H_2$ was utilized for the complete reduction of the unreduced active metal species in the catalyst at 850 ℃ [22,83]. Normal reduction time for a catalyst is about 3–4 h but in this case catalyst support, BFA is the mix matrix of various metal oxides in contrast to other support materials which are either a single metal oxide or a proper combination of multiple oxides, that is why the reduction time was higher as compared to conventional catalyst's support and of course exsolution process takes longer time than simple activation of catalyst. The catalytic activity initially shows a gradual increase in its value for the first 12 h and then catalyst activity remains stable continuously for the other 34 h as shown in Fig. 11. In the stability analysis maximum, $CH_4$ conversion was observed 88.5%,

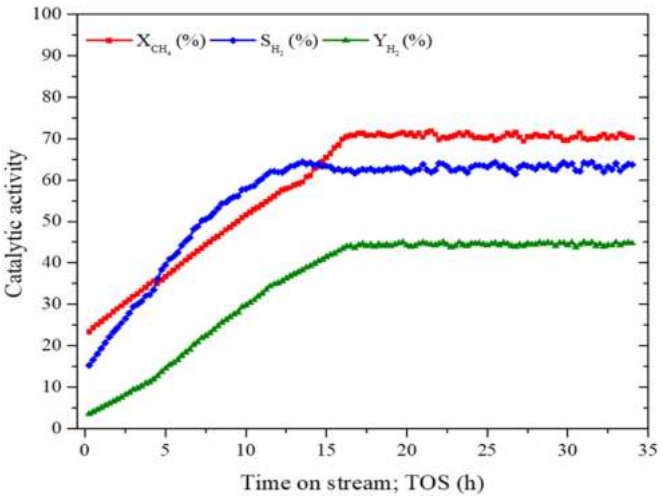


**Fig. 11.** Stability analysis of Co/$CeO_2$-BFA catalyst and TOS effect on $CH_4$ conversion, $H_2$ selectivity and yield at reaction at temperature = 850 °C, catalyst loading = 0.5 g and $CH_4$ flow rate = 20 mL $min^{-1}$.

similarly, $H_2$ selectivity and yield are recorded as 55.9% and 48.6% respectively for 34 h′ time on stream. The lower value of $H_2$ yield with respect to $CH_4$ conversion is attributed to the possible formation of certain higher hydrocarbons, mainly due to some site reaction followed via Fe activation [45,84]. The balance of the reaction is attributed to $C_xH_x$ gases which were not identified in this specific case due to the limitation of GC-TCD equipment. The catalyst stability enhanced not only due to Co-activation but the exsolution process of Fe and Co, which allows expanding with the carbon nanotubes [41,85,86]. The solid carbon deposited in thermal decomposition behaves as the catalyst support because BFA is the mix matrix of different oxides, following the metal exsolution process which improved the metal active sites [87,88].

### 3.3. Physicochemical properties of spent catalyst

Physicochemical properties of the spent catalyst have been carried out after 34 h of TOS. The SEM, XRD, TGA and EDS techniques are used to study the deposition of carbon over spent catalyst. The SEM morphology of the spent catalyst is shown in Fig. 12(a,b). Morphology of spent $Co/CeO_2$-BFA has been changed as compared to fresh nanocomposite which clearly shows deposition of graphite carbon nanotubes over BFA micro-flakes [89] which was later confirmed with the XRD study.

The spent catalyst XRD pattern is shown in Fig. 12(c). XRD confirms the formation of hexagonal graphite carbon (JCPDF# 26-1079) is recorded at $2\theta = 26.6^\circ$ with hkl (003). The cubic structured $CeO_2$ (JCPDF# 49-1415) having phase (012) was also detected at an angle of 43.9°, whose structure has been changed due to the reason that catalyst was heated for 34 h at 850 ℃, in the reaction where carbon was exulted from support and enhance the activity. The TGA profile of deposited carbon is shown in Fig. 12(d). TGA of spent catalyst performed in air environment which shows a major weight loss of about 69% in the range 530–680 ℃. The weight loss is majorly attributed to the combustion of graphitic carbon in the air. The weight of the deposited carbon during the 34 h TOS was calculated 6.3 g which was calculated by subtracting weight of loaded reactor before start of reaction from weight of reactor after reaction completion. The remaining carbon balance from theoritical calculation is ascribed to the possible formation of $C_xH_x$ species.

EDX spectrum of spent catalyst is shown in Fig. 13 which shows the major peaks for carbon with 61.8% by weight and other peaks were observed for Al, Si, Ca, and Fe. An element like Al, Si, Ca and Fe are the major constituents of the BFA while carbon has been deposited over the catalyst surface which suppressed the Co and $CeO_2$ concentration.

## 4. Conclusion

The $Co/CeO_2$-BFA nanocomposite is synthesized successfully and applied in methane decomposition. The characterizations revealed that catalyst has suitable physicochemical properties with the advantages of crystalline structure, micro flakes morphology, and high stability up to 850 ℃. The addition of Co as active metal over BFA and synthesized with $CeO_2$ nanowires further enhanced the catalytic performance in terms of catalyst stability, $CH_4$ conversion, $H_2$ selectivity, and yield. The maximum $CH_4$ conversion was 88%, $H_2$ selectivity and yield were 55.9%

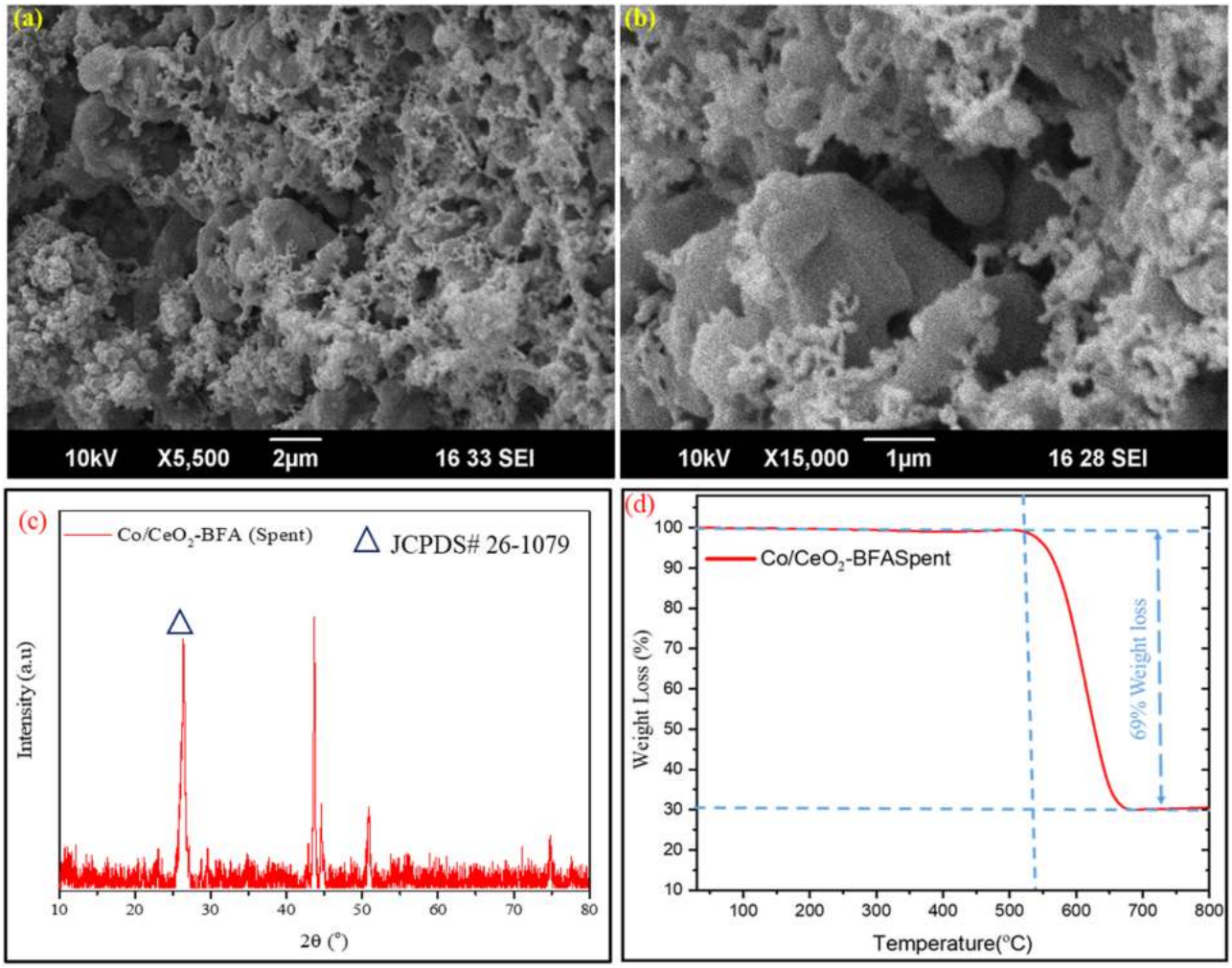


**Fig. 12.** (a,b) SEM micrograph of spent $Co/CeO_2$-BFA, (c) XRD of $Co/CeO_2$-BFA-spent and (d) TGA of $Co/CeO_2$-BFA-spent on air environment.

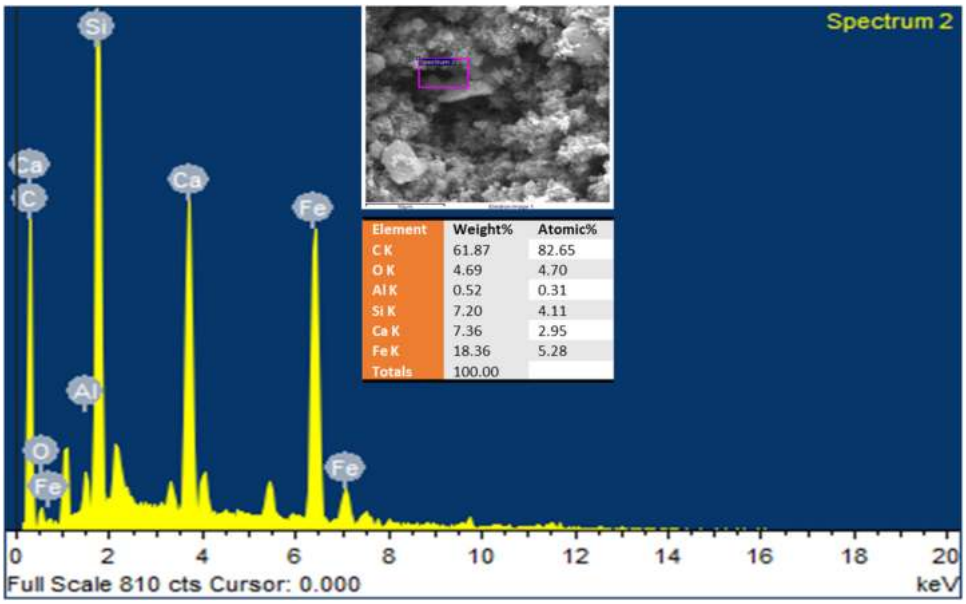


**Fig. 13.** EDS analysis of spent Co/$CeO_2$-BFA after 34 h TOS.

and 48.65%, respectively for 5% Co/$CeO_2$-BFA catalyst. The stability analysis was investigated for 34 h without compromising $CH_4$ conversion, $H_2$ selectivity, and yield. The obtained results show that biomass fly ash derived catalyst for catalytic application is an economical approach and the direct employment of BFA as catalyst support reduces the synthesis cost of a heterogeneous catalyst.

## CRediT authorship contribution statement

**Jehangeer Raza:** Conceptualization, Methodology, **Asif Hussain Khoja**: Conceptualization, Methodology, Writing-original draft. **Salman Raza Naqvi**, **Muhammad taqi Mehran**: Writing-original draft. **Sehar Shakir, Rabia Liaquat**: Methodology and Writing-original draft. **Muhammad Tahir** and **Ghulam Ali**: Writing-original draft and Review revised draft.

## Declaration of Competing Interest

The authors declare that they have no known competing financial interests or personal relationships that could have appeared to influence the work reported in this paper.

## Acknowledgement

The authors acknowledge USPCAS-E NUST for laboratory facilities. The authors extended thanks to Mr Qamar-Ud-Din, (Lab Technologist) for his support in lab activities.

## References

[1] J.X. Qian, T.W. Chen, L.R. Enakonda, D.B. Liu, G. Mignani, J.-M. Basset, L. Zhou, Methane decomposition to produce CO-free hydrogen and nano-carbon over metal catalysts: a review, Int. J. Hydrog. Energy 45 (2020) 7981–8001.
[2] J.X. Qian, T.W. Chen, L.R. Enakonda, D.B. Liu, J.-M. Basset, L. Zhou, Methane decomposition to pure hydrogen and carbon nano materials: state-of-the-art and future perspectives, Int. J. Hydrog. Energy 45 (2020) 15721–15743.
[3] F. Dawood, M. Anda, G.M. Shafiullah, Hydrogen production for energy: an overview, Int. J. Hydrog. Energy 45 (2020) 3847–3869.
[4] U.P.M. Ashik, W.M.A. Wan Daud, H.F. Abbas, Production of greenhouse gas free hydrogen by thermocatalytic decomposition of methane – a review, Renew. Sustain. Energy Rev. 44 (2015) 221–256.
[5] L. Weger, A. Abanades, T. Butler, Methane cracking as a bridge technology to the hydrogen economy, Int. J. Hydrog. Energy 42 (2017) 720–731.
[6] IEA, CO2 Emissions from Fuel Combustion 2020, International Energy Agency 2021.
[7] A.S. Al-Fatesh, A.H. Fakeeha, W.U. Khan, A.A. Ibrahim, S.B. He, K. Seshan, Production of hydrogen by catalytic methane decomposition over alumina supported mono-, bi- and tri-metallic catalysts, Int. J. Hydrog. Energy 41 (2016) 22932–22940.
[8] M. Karaismailoglu, H.E. Figen, S.Z. Baykara, Hydrogen production by catalytic methane decomposition over yttria doped nickel based catalysts, Int. J. Hydrog. Energy 44 (2019) 9922–9929.
[9] A.H. Khoja, M. Tahir, N.A.S. Amin, Recent developments in non-thermal catalytic DBD plasma reactor for dry reforming of methane, Energy Convers. Manag. 183 (2019) 529–560.
[10] A.H. Khoja, M. Tahir, N.A. Saidina Amin, Process optimization of DBD plasma dry reforming of methane over Ni/$La_2O_3$-$MgAl_2O_4$ using multiple response surface methodology, Int. J. Hydrog. Energy 44 (2019) 11774–11787.
[11] M. Usman, W.W. Daud, Recent advances in the methanol synthesis via methane reforming processes, RSC Adv. 5 (2015) 21945–21972.
[12] V. Havran, M.P. Dudukovic, C.S. Lo, Conversion of methane and carbon dioxide to higher value products, Ind. Eng. Chem. Res. 50 (2011) 7089–7100.
[13] N.P. Brandon, Z. Kurban, Clean energy and the hydrogen economy, Philos. Trans. A Math. Phys. Eng. Sci. 375 (2017), 20160400.
[14] A. Sartbaeva, V. Kuznetsov, S. Wells, P. Edwards, Hydrogen nexus in a sustainable energy future, Energy Environ. Sci. 1 (2008) 79–85.
[15] A.H. Khoja, M. Anwar, S. Shakir, M.T. Mehran, A. Mazhar, A. Javed, N.A.S. Amin, Thermal dry reforming of methane over $La_2O_3$ co-supported Ni/$MgAl_2O_4$ catalyst for hydrogen-rich syngas production, Res. Chem. Intermed. 46 (2020) 3817–3833.
[16] R.R.C.M. Silva, H.A. Oliveira, A.C.P.F. Guarino, B.B. Toledo, M.B.T. Moura, B.T. M. Oliveira, F.B. Passos, Effect of support on methane decomposition for hydrogen production over cobalt catalysts, Int. J. Hydrog. Energy 41 (2016) 6763–6772.
[17] K. Srilatha, D. Dheeravath, S.S. Kumar, H. Vurimindi, Sustainable fuel production by thermocatalytic decomposition of methane using Ni/ZnO catalyst, Nano Trends J. Nanotechnol. Appl. 19 (2017), 973-418.
[18] C. García-Sancho, R. Guil-López, A. Sebastián-López, R.M. Navarro, J.L.G. Fierro, Hydrogen production by methane decomposition: a comparative study of supported and bulk ex-hydrotalcite mixed oxide catalysts with Ni, Mg and Al, Int. J. Hydrog. Energy 43 (2018) 9607–9621.
[19] A.A. Ibrahim, A.H. Fakeeha, A.S. Al-Fatesh, A.E. Abasaeed, W.U. Khan, Methane decomposition over iron catalyst for hydrogen production, Int. J. Hydrog. Energy 40 (2015) 7593–7600.
[20] D. Kang, J.W. Lee, Enhanced methane decomposition over nickel–carbon–$B_2O_3$ core–shell catalysts derived from carbon dioxide, Appl. Catal. B Environ. 186 (2016) 41–55.
[21] H. Nishii, D. Miyamoto, Y. Umeda, H. Hamaguchi, M. Suzuki, T. Tanimoto, T. Harigai, H. Takikawa, Y. Suda, Catalytic activity of several carbons with different structures for methane decomposition and by-produced carbons, Appl. Surf. Sci. 473 (2019) 291–297.
[22] M. Pudukudy, Z. Yaakob, Methane decomposition over Ni, Co and Fe based monometallic catalysts supported on sol gel derived SiO2 microflakes, Chem. Eng. J. 262 (2015) 1009–1021.
[23] E. Tezel, H.E. Figen, S.Z. Baykara, Hydrogen production by methane decomposition using bimetallic Ni–Fe catalysts, Int. J. Hydrog. Energy 44 (2019) 9930–9940.
[24] J.B. Zhang, W.T. Xie, X. Li, Q.Q. Hao, H.Y. Chen, X.X. Ma, Methane decomposition over Ni/carbon catalysts prepared by selective gasification of coal char, Energy Convers. Manag. 177 (2018) 330–338.

[25] N. Bayat, F. Meshkani, M. Rezaei, Thermocatalytic decomposition of methane to $CO_x$-free hydrogen and carbon over Ni–Fe–Cu/$Al_2O_3$ catalysts, Int. J. Hydrog. Energy 41 (2016) 13039–13049.

[26] N. Bayat, M. Rezaei, F. Meshkani, Hydrogen and carbon nanofibers synthesis by methane decomposition over Ni–Pd/$Al_2O_3$ catalyst, Int. J. Hydrog. Energy 41 (2016) 5494–5503.

[27] A. Wolfbeisser, G. Kovacs, S.M. Kozlov, K. Fottinger, J. Bernardi, B. Klotzer, K. M. Neyman, G. Rupprechter, Surface composition changes of CuNi-$ZrO_2$ during methane decomposition: an operando NAP-XPS and density functional study, Catal. Today 283 (2017) 134–143.

[28] H.F. Abbas, W.M.A. Wan Daud, Hydrogen production by methane decomposition: a review, Int. J. Hydrog. Energy 35 (2010) 1160–1190.

[29] A.H. Fakeeha, A.A. Ibrahim, W.U. Khan, K. Seshan, R.L. Al Otaibi, A.S. Al-Fatesh, Hydrogen production via catalytic methane decomposition over alumina supported iron catalyst, Arab. J. Chem. 11 (2018) 405–414.

[30] M. Pudukudy, Z. Yaakob, Q.M. Jia, M.S. Takriff, Catalytic decomposition of methane over rare earth metal (Ce and La) oxides supported iron catalysts, Appl. Surf. Sci. 467 (2019) 236–248.

[31] A.H. Khoja, A. Azad, F. Saleem, B.A. Khan, S.R. Naqvi, M.T. Mehran, N.A.S. Amin, Hydrogen production from methane cracking in dielectric barrier discharge catalytic plasma reactor using a nanocatalyst, Energies 13 (2020) 5921.

[32] L. Zhou, L.R. Enakonda, M. Harb, Y. Saih, A. Aguilar-Tapia, S. Ould-Chikh, J. L. Hazemann, J. Li, N. Wei, D. Gary, P. Del-Gallo, J.M. Basset, Fe catalysts for methane decomposition to produce hydrogen and carbon nano materials, Appl. Catal. B Environ. 208 (2017) 44–59.

[33] M. Pudukudy, Z. Yaakob, M.S. Takriff, Methane decomposition into COx free hydrogen and multiwalled carbon nanotubes over ceria, zirconia and lanthana supported nickel catalysts prepared via a facile solid state citrate fusion method, Energy Convers. Manag. 126 (2016) 302–315.

[34] M.S. Tian, K.Z. Li, X. Zhu, Y.G. Wei, Y.N. Zheng, L. Zhang, Y.H. Long, H. Wang, Modified Al@$Al_2O_3$ phase change materials by carbon via in-situ catalytic decomposition of methane, Sol. Energy Mater. Sol. Cells 200 (2019), 109924.

[35] A.E. Awadallah, D.S. El-Desouki, S.M. Abdel-Azim, N.A.K. Aboul-Gheit, S. M. Abdel-Hamid, A.K. Aboul-Gheit, Effect of La, Ce and Nd oxides addition on the activity and stability of Co/MgO catalyst for methane decomposition into COx-free $H_2$ production and carbon nanotubes, Fuller. Nanotub. Carbon Nanostruct. 26 (2018) 525–534.

[36] J.C. Araújo, L.F. Oton, B. Bessa, A.B. Neto, A.C. Oliveira, R. Lang, L. Otubo, J. M. Bueno, The role of Pt loading on $La_2O_3$-$Al_2O_3$ support for methane conversion reactions via partial oxidation and steam reforming, Fuel 254 (2019), 115681.

[37] A.E. Awadallah, M.S. Mostafa, A.A. Aboul-Enein, S.A. Hanafi, Hydrogen production via methane decomposition over Al2O3–TiO2 binary oxides supported Ni catalysts: effect of Ti content on the catalytic efficiency, Fuel 129 (2014) 68–77.

[38] W.O. Alabi, K.O. Sulaiman, H. Wang, Sensitivity of the properties and performance of Co catalyst to the nature of support for $CO_2$ reforming of CH4, Chem. Eng. J. 390 (2020), 124486.

[39] S. Chen, J. Zaffran, B. Yang, Dry reforming of methane over the cobalt catalyst: theoretical insights into the reaction kinetics and mechanism for catalyst deactivation, Appl. Catal. B Environ. 270 (2020), 118859.

[40] G. Italiano, A. Delia, C. Espro, G. Bonura, F. Frusteri, Methane decomposition over Co thin layer supported catalysts to produce hydrogen for fuel cell, Int. J. Hydrog. Energy 35 (2010) 11568–11575.

[41] H.D. Setiabudi, C.C. Chong, S. Abed, L. Teh, S. Chin, Comparative study of Ni-Ce loading method: beneficial effect of ultrasonic-assisted impregnation method in $CO_2$ reforming of $CH_4$ over Ni-Ce/SBA-15, J. Environ. Chem. Eng. 6 (2018) 745–753.

[42] Y. Gao, J. Jiang, Y. Meng, A. Aihemaiti, T. Ju, X. Chen, F. Yan, A novel nickel catalyst supported on activated coal fly ash for syngas production via biogas dry reforming, Renew. Energy 149 (2020) 786–793.

[43] C. Zhao, L. Yang, S. Xing, W. Luo, Z. Wang, P. Lv, Biodiesel production by a highly effective renewable catalyst from pyrolytic rice husk, J. Clean. Prod. 199 (2018) 772–780.

[44] R. Shan, L. Lu, Y. Shi, H. Yuan, J. Shi, Catalysts from renewable resources for biodiesel production, Energy Convers. Manag. 178 (2018) 277–289.

[45] M. Assad Munawar, A. Hussain Khoja, M. Hassan, R. Liaquat, S. Raza Naqvi, M. Taqi Mehran, A. Abdullah, F. Saleem, Biomass ash characterization, fusion analysis and its application in catalytic decomposition of methane, Fuel 285 (2021), 119107.

[46] A.R.K. Gollakota, V. Volli, C.M. Shu, Progressive utilisation prospects of coal fly ash: a review, Sci. Total Environ. 672 (2019) 951–989.

[47] F. Goodarzi, Characteristics and composition of fly ash from Canadian coal-fired power plants, Fuel 85 (2006) 1418–1427.

[48] S.R. Wang, F. Zhang, Q.J. Cai, X.B. Li, L.J. Zhu, Q. Wang, Z.Y. Luo, Catalytic steam reforming of bio-oil model compounds for hydrogen production over coal ash supported Ni catalyst, Int. J. Hydrog. Energy 39 (2014) 2018–2025.

[49] M. Shahbaz, S. Yusup, A. Inayat, D.O. Patrick, A. Pratama, M. Ammar, Optimization of hydrogen and syngas production from PKS gasification by using coal bottom ash, Bioresour. Technol. 241 (2017) 284–295.

[50] A.S. Al-Rahbi, P.T. Williams, Waste ashes as catalysts for the pyrolysis–catalytic steam reforming of biomass for hydrogen-rich gas production, J. Mater. Cycles Waste Manag. 21 (2019) 1224–1231.

[51] T. Zhu, M. Flytzani-Stephanopoulos, Catalytic partial oxidation of methane to synthesis gas over Ni–$CeO_2$, Appl. Catal. A Gen. 208 (2001) 403–417.

[52] N. Laosiripojana, W. Sutthisripok, S. Assabumrungrat, Synthesis gas production from dry reforming of methane over $CeO_2$ doped Ni/$Al_2O_3$: influence of the doping ceria on the resistance toward carbon formation, Chem. Eng. J. 112 (2005) 13–22.

[53] W. Ahmed, A.E. Awadallah, A.A. Aboul-Enein, Ni/CeO2–Al2O3 catalysts for methane thermo-catalytic decomposition to CO -free H2 production, Int. J. Hydrog. Energy 41 (2016) 18484–18493.

[54] A.H. Khoja, M. Tahir, N.A. Saidina Amin, Evaluating the performance of a Ni catalyst supported on $La_2O_3$-$MgAl_2O_4$ for dry reforming of methane in a packed bed dielectric barrier discharge plasma reactor, Energy Fuels 33 (2019) 11630–11647.

[55] A.H. Khoja, M. Tahir, N.A.S. Amin, Cold plasma dielectric barrier discharge reactor for dry reforming of methane over Ni/ɤ-$Al_2O_3$ -MgO nanocomposite, Fuel Process. Technol. 178 (2018) 166–179.

[56] A.H. Khoja, M. Tahir, N.A.S. Amin, A. Javed, M.T. Mehran, Kinetic study of dry reforming of methane using hybrid DBD plasma reactor over $La_2O_3$ co-supported $Ni/MgAl_2O_4$ catalyst, Int. J. Hydrog. Energy 45 (2020) 12256–12271.

[57] H. Wang, W. Cui, Xa Dong, J. Li, Q. Chen, Z. Wang, Y. Sun, J. Sheng, Y. Zhou, Y. Zhang, F. Dong, Interfacial activation of reactants and intermediates on $CaSO_4$ insulator-based heterostructure for efficient photocatalytic NO removal, Chem. Eng. J. 390 (2020), 124609.

[58] X. Zhang, J. Huang, Z. Kang, D.-P. Yang, R. Luque, Eggshell-templated synthesis of PbS/$CaCO_3$ nanocomposites for $CO_3$− mediated efficient degradation of tetracycline under solar light irradiation, Mol. Catal. 484 (2020), 110786.

[59] A. Kumar, M.K. Naskar, Single-step process without organic template for the formation of zeolite A from RHA, Int. J. Appl. Ceram. Technol. 16 (2019) 1525–1532.

[60] Y. Wang, J. Ma, S. Zuo-Jiang, K. Chen, Tailorable magnetic properties of ε-$Fe_2O_3$/$SiO_2$ hybrid via alkaline etching, Ceram. Int. 43 (2017) 16482–16487.

[61] W. Nabgan, T.A. Tuan Abdullah, R. Mat, B. Nabgan, Y. Gambo, K. Moghadamian, Acetic acid-phenol steam reforming for hydrogen production: effect of different composition of $La_2O_3$-$Al_2O_3$ support for bimetallic Ni-Co catalyst, J. Environ. Chem. Eng. 4 (2016) 2765–2773.

[62] A.I. Paksoy, B.S. Caglayan, E. Ozensoy, A.N. Ökte, A.E. Aksoylu, The effects of Co/Ce loading ratio and reaction conditions on CDRM performance of Co Ce/$ZrO_2$ catalysts, Int. J. Hydrog. Energy 43 (2018) 4321–4334.

[63] A.Y. Khodakov, Fischer-Tropsch synthesis: relations between structure of cobalt catalysts and their catalytic performance, Catal. Today 144 (2009) 251–257.

[64] J. Valencia, N. Arias-Duque, O. Giraldo, A. Rosales-Rivera, Synthesis and characterization of magnesium-doped layered manganese oxides, Rev. Mex. Fís. 58 (2012) 151–154.

[65] R.P. dos Santos, J. Martins, C. Gadelha, B. Cavada, A.V. Albertini, F. Arruda, M. Vasconcelos, E. Teixeira, F. Alves, J. Lima Filho, V. Freire, Coal fly ash ceramics: preparation, characterization, and use in the hydrolysis of sucrose, ScientificWorldJournal 2014 (2014), 154651.

[66] M. El-Hagary, E.R. Shaaban, S.H. Moustafa, G.M.A. Gad, The particle size-dependent optical band gap and magnetic properties of Fe-doped $CeO_2$ nanoparticles, Solid State Sci. 91 (2019) 15–22.

[67] J. Temuujin, U. Bayarzula, E. Surenjav, K.D. Sung, C.Y. Sik, Influence of cerium oxide ($CeO_2$) addition on the mechanical properties of glass ceramics precursor prepared from fly ash, J. Ceram. Process. Res. 18 (2017) 112–115.

[68] S. Khajeh Talkhoncheh, M. Haghighi, Syngas production via dry reforming of methane over Ni-based nanocatalyst over various supports of clinoptilolite, ceria and alumina, J. Nat. Gas Sci. Eng. 23 (2015) 16–25.

[69] M.Y. Cui, X.Q. Yao, W.J. Dong, K. Tsukamoto, C.R. Li, Template-free synthesis of CuO–$CeO_2$ nanowires by hydrothermal technology, J. Cryst. Growth 312 (2010) 287–293.

[70] C.M. Kalamaras, A.M. Efstathiou, Hydrogen Production Technologies: Current State and Future Developments, Conference Papers in Energy, 2013 (2013) 1–9.

[71] M.L. Dos Santos, R.C. Lima, C.S. Riccardi, R.L. Tranquilin, P.R. Bueno, J.A. Varela, E. Longo, Preparation and characterization of ceria nanospheres by microwave-hydrothermal method, Mater. Lett. 62 (2008) 4509–4511.

[72] J. Kalembkiewicz, D. Galas, E. Sitarz-Palczak, The physicochemical properties and composition of biomass ash and evaluating directions of its applications, Pol. J. Environ. Stud. 27 (2018) 2593–2603.

[73] W. Mozgawa, M. Krol, J. Dyczek, J. Deja, Investigation of the coal fly ashes using IR spectroscopy, Spectrochim. Acta A Mol. Biomol. Spectrosc. 132 (2014) 889–894.

[74] Y.A. Syed Khadar, A. Balamurugan, V.P. Devarajan, R. Subramanian, S. Dinesh Kumar, Synthesis, characterization and antibacterial activity of cobalt doped cerium oxide ($CeO_2$:Co) nanoparticles by using hydrothermal method, J. Mater. Res. Technol. 8 (2019) 267–274.

[75] M.T. Farid, I. Ahmad, S. Aman, M. Kanwal, G. Murtaza, I.Ali, M. Ishfaq, SEM, FTIR and dielectric properties of cobalt substituted spinel ferrites, 2015.

[76] W. Girma, I. Diaz, Encapsulation of Co (II) Complex with A Schiff Base Ligands Derived from 1, 10-Phenantroline-5, 6-Dione and O-Phenylene Diamine in Zeolite Y, 2016.

[77] V. Ramasubramanian, H. Ramsurn, G.L. Price, Hydrogen production by catalytic decomposition of methane over Fe based bi-metallic catalysts supported on $CeO_2$–$ZrO_2$, Int. J. Hydrog. Energy 45 (2020) 12026–12036.

[78] N.A. Pechimuthu, K.K. Pant, S.C. Dhingra, Deactivation studies over Ni−K/$CeO_2$−$Al_2O_3$ catalyst for dry reforming of methane, Ind. Eng. Chem. Res. 46 (2007) 1731–1736.

[79] P. Jiang, Y. Shang, T. Cheng, Y. Bi, K. Shi, S. Wei, G. Xu, K. Zhen, Methane decomposition over Ni/α-$Al_2O_3$ promoted by $La_2O_3$ and $CeO_2$, J. Nat. Gas Chem. 12 (2003) 183–188.

[80] F.-J. Spiess, S.L. Suib, K. Irie, Y. Hayashi, H. Matsumoto, Metal effect and flow rate effect in the hydrogen production from methane, Catal. Today 89 (2004) 35–45.

[81] H. Zhang, C. Du, A. Wu, Z. Bo, J. Yan, X. Li, Rotating gliding arc assisted methane decomposition in nitrogen for hydrogen production, Int. J. Hydrog. Energy 39 (2014) 12620–12635.

[82] A.H. Khoja, M. Tahir, N.A.S. Amin, Dry reforming of methane using different dielectric materials and DBD plasma reactor configurations, Energy Convers. Manag. 144 (2017) 262–274.
[83] A.E. Awadallah, A.A. Aboul-Enein, D.S. El-Desouki, A.K. Aboul-Gheit, Catalytic thermal decomposition of methane to COx-free hydrogen and carbon nanotubes over MgO supported bimetallic group VIII catalysts, Appl. Surf. Sci. 296 (2014) 100–107.
[84] A. Holmen, O. Olsvik, O.A. Rokstad, Pyrolysis of natural gas: chemistry and process concepts, Fuel Process. Technol. 42 (1995) 249–267.
[85] A. Leba, R. Yıldırım, Determining most effective structural form of nickel-cobalt catalysts for dry reforming of methane, Int. J. Hydrog. Energy 45 (2020) 4268–4283.
[86] A.S. Al-Fatesh, A.H. Fakeeha, A.A. Ibrahim, W.U. Khan, H. Atia, R. Eckelt, K. Seshan, B. Chowdhury, Decomposition of methane over alumina supported Fe and Ni–Fe bimetallic catalyst: effect of preparation procedure and calcination temperature, J. Saudi Chem. Soc. 22 (2018) 239–247.
[87] C. Tang, K. Kousi, D. Neagu, J. Portoles, E.I. Papaioannou, I.S. Metcalfe, Towards efficient use of noble metals via exsolution exemplified for CO oxidation, Nanoscale 11 (2019) 16935–16944.
[88] D. Zubenko, S. Singh, B.A. Rosen, Exsolution of Re-alloy catalysts with enhanced stability for methane dry reforming, Appl. Catal. B Environ. 209 (2017) 711–719.
[89] T.J. Siang, S. Singh, O. Omoregbe, L.G. Bach, N.H.H. Phuc, D.-V.N. Vo, Hydrogen production from $CH_4$ dry reforming over bimetallic Ni–Co/$Al_2O_3$ catalyst, J. Energy Inst. 91 (2018) 683–694.